Conference Applications of Mathematics 2012
in honor of the 60th birthday of Michal Křížek.
Institute of Mathematics AS CR, Prague 2012

NUMERICAL COMPARISON OF UNSTEADY COMPRESSIBLE VISCOUS FLOW IN CONVERGENT CHANNEL

Petra Pořízková[1], Karel Kozel[2], Jaromír Horáček[2]

[1] Czech Technical University in Prague, Faculty of Mechanical Engineering
Department of Technical Mathematics
Karlovo nám. 13, CZ 121 35 Prague, Czech Republic
puncocha@marian.fsik.cvut.cz
[2] Institute of Thermomechanics AS CR, Centre of Energetics
Dolejškova 5, CZ 182 00 Prague, Czech Republic
kozelk@fsik.cvut.cz, jaromirh@it.cas.cz

Abstract

This study deals with a numerical solution of a 2D flows of a compressible viscous fluids in a convergent channel for low inlet airflow velocity. Three governing systems – *Full system, Adiabatic system, Iso-energetic system* based on the Navier-Stokes equations for laminar flow are tested. The numerical solution is realized by finite volume method and the predictor-corrector MacCormack scheme with Jameson artificial viscosity using a grid of quadrilateral cells. The unsteady grid of quadrilateral cells is considered in the form of conservation laws using Arbitrary Lagrangian-Eulerian method.

The numerical results, acquired from a developed program, are presented for inlet velocity $\hat{u}_\infty = 4.12\text{ms}^{-1}$ and Reynolds number $\text{Re} = 4 \times 10^3$.

1. Introduction

A current challenging question is a mathematical and physical description of the mechanism for transforming the airflow energy in human vocal tract (convergent channel) into the acoustic energy representing the voice source in humans. The voice source signal travels from the glottis to the mouth, exciting the acoustic supraglottal spaces, and becomes modified by acoustic resonance properties of the vocal tract [1]. The airflow coming from the lungs causes self-oscillations of the vocal folds, and the glottis completely closes in normal phonation regimes, generating acoustic pressure fluctuations. In this study, the movement of the boundary channel is known, harmonically opening and nearly closing in the narrowest cross-section of the channel, making the investigation of the airflow field in the glottal region possible. For phonation of vowels, the frequencies of the vocal folds oscillations are in the region from

cc 82 Hz for bass up to cc 1170 Hz for soprano in singing voice, the airflow velocity in the trachea is approximately in the range of 0.3-5.2 ms^{-1} taking into account the tracheal diameter in humans in the range 14.5-17.6 mm [2].

Acoustic wave propagation in the vocal tract is usually modeled from incompressible flow models separately using linear acoustic perturbation theory, the wave equation for the potential flow [2] or the Light-hill approach on sound generated aerodynamically [3].

Goal of this work is numerical simulation of compressible viscous flow in 2D convergent channel which involves attributes of real flow causing acoustic perturbations as is "Coandă phenomenon" (the tendency of a fluid jet to be attracted to a nearby surface), vortex convection and diffusion, jet flapping etc. along with lower call on computer time, due to later extension in 3D channel flow.

2. Governing equations

The 2D system of Navier-Stokes equations has been used as mathematical model to describe the unsteady laminar flow of the compressible viscous fluid in a domain. The system of Navier-Stokes equations is expressed in non-dimensional conservative form [4]:

$$\frac{\partial \mathbf{W}}{\partial t} + \frac{\partial \mathbf{F}}{\partial x} + \frac{\partial \mathbf{G}}{\partial y} = \frac{1}{\mathrm{Re}} \left(\frac{\partial \mathbf{R}}{\partial x} + \frac{\partial \mathbf{S}}{\partial y} \right). \tag{1}$$

$\mathbf{W}$ is the vector of conservative variables $\mathbf{W} = [\rho, \rho u, \rho v, e]^T$ where ρ denotes density, u and v are the components of the velocity vector and e is the total energy per unit volume. $\mathbf{F}$ and $\mathbf{G}$ are the vectors of inviscid fluxes and $\mathbf{R}$, $\mathbf{S}$ are the vectors of viscous fluxes. The static pressure p in $\mathbf{F}$ and $\mathbf{G}$ is expressed by the state equation in the form

$$p = (\kappa - 1) \left[e - \frac{1}{2} \rho \left(u^2 + v^2 \right) \right], \tag{2}$$

where $\kappa = 1.4$ is the ratio of specific heats.

The transformation to the non-dimensional form uses inflow parameters (marked with the infinity subscript) as reference variables (dimensional variables are marked with the hat): the speed of sound $\hat{c}_\infty = 343$ ms^{-1}, density $\hat{\rho}_\infty = 1.225$ kg m^{-3}, temperature $\hat{T}_\infty = 293.15$ K, dynamic viscosity $\hat{\eta}_\infty = 18 \cdot 10^{-6}$ Pa $\cdot$ s and a reference length $\hat{L}_r = 0.02$ m.

General Reynolds number in (1) is computed from reference variables $\mathrm{Re} = \hat{\rho}_\infty \hat{c}_\infty \hat{L}_r / \hat{\eta}_\infty$. The non-dimensional dynamic viscosity in the dissipative terms is a function of temperature in the form $\eta = (T/T_\infty)^{3/4}$.

The system of equations (1) and (2) is so-called *Full system*. We present two other governing systems of equations based on the Navier-Stokes equations (1), depend on expression of state equation for static pressure p which is depend on energy flow condition in the system. The second governing system is so-called *Adiabatic system*

$$p = \frac{1}{\kappa} \rho^\kappa, \tag{3}$$

and third governing system is so-called *Iso-energetic system*

$$p = \frac{\rho}{\kappa}\left[1 + \frac{\kappa - 1}{2}\left(\frac{\hat{u}_\infty}{\hat{c}_\infty}\right)^2 - \frac{\kappa - 1}{2}(u^2 + v^2)\right]. \tag{4}$$

Both last systems have the pressure expression independent on variable e and the system (1) is reduced on the first three equations.

2.1. Computational domain and boundary conditions

The bounded computational domain D_1 used for the numerical solution of flow field in the channel is shown in Figure 1. The domain is symmetric channel, the shape of which is inspired by the shape of the trachea (inlet part), vocal folds, false vocal folds and supraglottal spaces (outlet part) in human vocal tract. The upper and the lower boundaries are the channel walls. A part of the walls changes its shape between the points A and B according to given harmonic function of time and axial coordinate (see [5]). The gap width is the narrowest part of the channel (in point C) and is oscillating between the minimum $g_{min} = 0.4$ mm and maximum $g_{max} = 2.8$ mm.

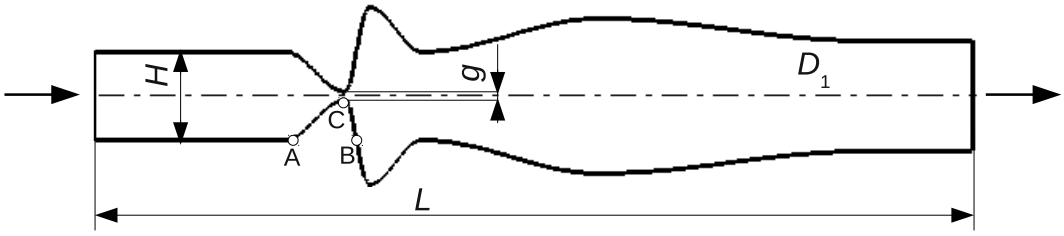

Figure 1: The computational domain D_1. $L = 8$ (160 mm), $H = 0.8$ (16 mm), $g = 0.08$ (1.6 mm) - middle position.

The boundary conditions are considered in the following formulation:

1. Upstream conditions: $u_\infty = \frac{\hat{u}_\infty}{\hat{c}_\infty}$; $v_\infty = 0$; $\rho_\infty = 1$; p_∞ is extrapolated from D_1.
2. Downstream conditions: $p_2 = 1/\kappa$; $(\rho, \rho u, \rho v)$ are extrapolated from D_1.
3. Flow on the wall: $(u, v) = (u_{wall}, v_{wall})$ and furthermore for *Full system* $\frac{\partial T}{\partial \vec{n}} = 0$. Vector (u_{wall}, v_{wall}) represents velocity of the channel walls and $T = \kappa p/\rho$ is the temperature.

The general Reynolds number in (1) is multiply with non-dimensional value $\frac{\hat{u}_\infty}{\hat{c}_\infty} H$ represents kinematic viscosity scale and for computation of the real problem inlet Reynolds number $\mathrm{Re}_\infty = \hat{\rho}_\infty \hat{c}_\infty \frac{\hat{u}_\infty}{\hat{c}_\infty} H \hat{L}_r / \hat{\eta}_\infty$ is used.

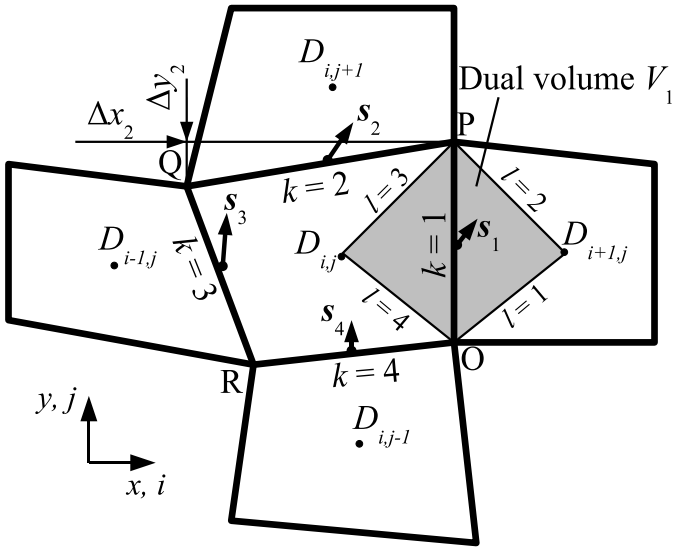

Figure 2: Finite volume $D_{i,j}$ and the dual volume V'_k.

3. Numerical solution

The numerical solution uses finite volume method (FVM) in cell centered form on the grid of quadrilateral cells, see e.g. [4]. In the time-changing domain, the integral form of FVM is derived using Arbitrary Lagrangian-Eulerian (ALE) formulation. The ALE method defines homomorphic mapping of the reference domain $D_{t=0}$ at initial time $t = 0$ to a domain D_t at $t > 0$ [6]. The explicit predictor-corrector MacCormack (MC) scheme in the domain with a moving grid of quadrilateral cells is used. The scheme is 2nd order accurate in time and space [4]:

$$\begin{aligned}
\mathbf{W}_{i,j}^{n+1/2} &= \frac{\mu_{i,j}^n}{\mu_{i,j}^{n+1}}\mathbf{W}_{i,j}^n - \frac{\Delta t}{\mu_{i,j}^{n+1}}\sum_{k=1}^{4}\left[\left(\tilde{\mathbf{F}}_k^n - s_{1k}\mathbf{W}_k^n - \frac{1}{Re}\tilde{\mathbf{R}}_k^n\right)\Delta y_k\right. \\
&- \left.\left(\tilde{\mathbf{G}}_k^n - s_{2k}\mathbf{W}_k^n - \frac{1}{Re}\tilde{\mathbf{S}}_k^n\right)\Delta x_k\right], \\
\overline{\mathbf{W}}_{i,j}^{n+1} &= \frac{\mu_{i,j}^n}{\mu_{i,j}^{n+1}}\frac{1}{2}\left(\mathbf{W}_{i,j}^n + \mathbf{W}_{i,j}^{n+1/2}\right) - \frac{\Delta t}{2\mu_{i,j}^{n+1}}\sum_{k=1}^{4}\left[\left(\tilde{\mathbf{F}}_k^{n+1/2} - s_{1k}\mathbf{W}_k^{n+1/2}\right.\right. \\
&- \left.\left.\frac{1}{Re}\tilde{\mathbf{R}}_k^{n+1/2}\right)\Delta y_k - \left(\tilde{\mathbf{G}}_k^{n+1/2} - s_{2k}\mathbf{W}_k^{n+1/2} - \frac{1}{Re}\tilde{\mathbf{S}}_k^{n+1/2}\right)\Delta x_k\right], \qquad (5)
\end{aligned}$$

$\Delta t = t^{n+1} - t^n$ is the time step, $\mu_{i,j} = \int\int_{D_{i,j}} dxdy$ is the volume of cell $D_{i,j}$, Δx and Δy are the steps of the grid in directions x and y, vector $\mathbf{s}_k = (s_1,\ s_2)_k$ represents the speed of edge k (see Figure 2). The physical fluxes $\mathbf{F}$, $\mathbf{G}$, $\mathbf{R}$, $\mathbf{S}$ on the edge k of the cell $D_{i,j}$ are replaced by numerical fluxes (marked with tilde) $\tilde{\mathbf{F}}$, $\tilde{\mathbf{G}}$, $\tilde{\mathbf{R}}$, $\tilde{\mathbf{S}}$ as approximations of the physical fluxes. The higher partial derivatives of velocity and temperature in $\tilde{\mathbf{R}}_k$, $\tilde{\mathbf{S}}_k$ are approximated using dual volumes V'_k (see [4]) as shown in Figure 2.

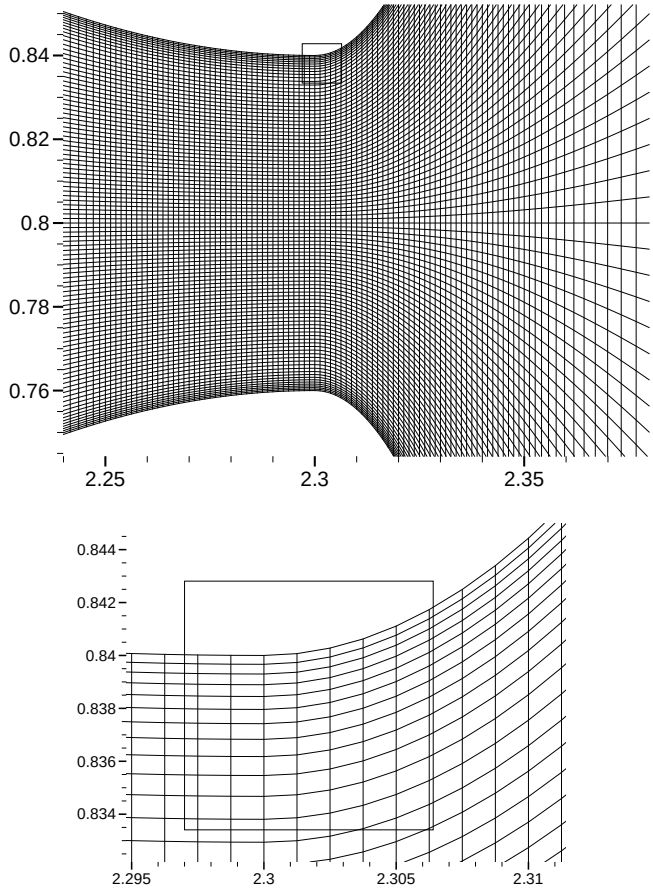

Figure 3: Mesh in domain D_1 - detail.

The last term used in the MC scheme is the Jameson artificial dissipation $AD(W_{i,j})^n$ [7], then the vector of conservative variables $\mathbf{W}$ can be computed at a new time level $\mathbf{W}_{i,j}^{n+1} = \overline{\mathbf{W}}_{i,j}^{n+1} + AD(W_{i,j})^n$.

The grid of the channel have successive refinement cells near the wall (see Figure 3). The minimum cell size in y - direction is $\Delta y_{min} \approx 1/\sqrt{\mathrm{Re}_\infty}$ to resolve capture boundary layer effects.

4. Numerical results

The numerical results were obtained (using a specifically developed program) for the following input data: uniform inflow ratio velocity $\frac{\hat{u}_\infty}{\hat{c}_\infty} = 0.012$ ($\hat{u}_\infty = 4.116$ ms^{-1}), Reynolds number $\mathrm{Re}_\infty = 4481$ and atmospheric pressure $p_2 = 1/\kappa$ ($\hat{p}_2 = 102942$ Pa) at the outlet. The computational domain contained 450×100 cells. The detail of the mesh near the gap is shown in Figure 3.

The computation has been carried out in two stages. First, a numerical solution

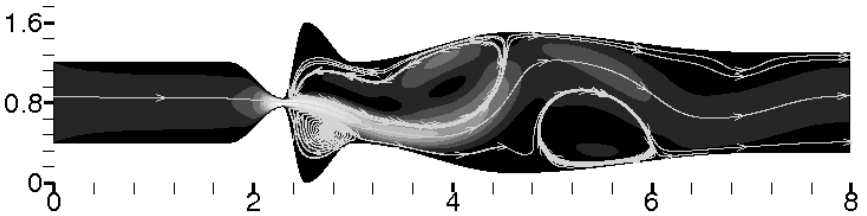

(a) *Full system*, $\frac{\hat{u}_{max}}{\hat{c}_\infty} = 0.177$

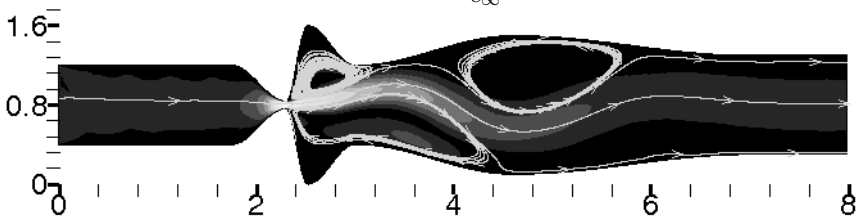

(b) *Adiabatic system*, $\frac{\hat{u}_{max}}{\hat{c}_\infty} = 0.166$

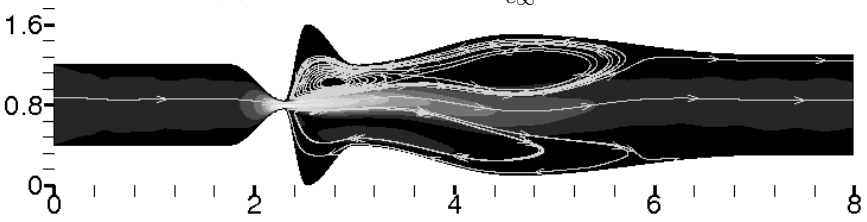

(c) *Iso-energetic system*, $\frac{\hat{u}_{max}}{\hat{c}_\infty} = 0.160$

Figure 4: Initial conditions in domain D_1 computed with the governing systems. $\frac{\hat{u}_\infty}{\hat{c}_\infty} = 0.012$, $\mathrm{Re}_\infty = 4481$, $p_2 = 1/\kappa$, mesh: 450×100. Results are mapped by iso-lines of ratio velocity and by streamlines.

is obtained, when the channel between points A and B has a rigid wall fixed in the middle position of the gap width (see Fig. 1). Then this solution is used as the initial condition for the unsteady simulation.

Figure 4 shows initial conditions of the flows in domain D_1 computed with the governing systems. The pictures display non-symmetric flow developed behind the narrowest channel cross-section. Figure 5 shows the convergences to the steady state solution computed using the L_2 norm of momentum residuals (ρu). The convergence depends on coefficients of artificial dissipation $AD(W_{i,j})^n$ making strong or weak numerical viscosity of the scheme and on governing system. The graphs indicates the non-stationary solution which is caused probably by eddies separated behind gap and floating away. Numerical solution computed with *Iso-energetic system* has the worst residuals.

Figures 6, 7, 8 show the unsteady flow fields computed with the governing systems in domain D_1. Simulation is captured in five time instants during one vibration period (in the fourth cycle of the wall oscillation). The highest absolute maximum velocity ratio during one vibration period is computed with *Full system* (Fig. 6)

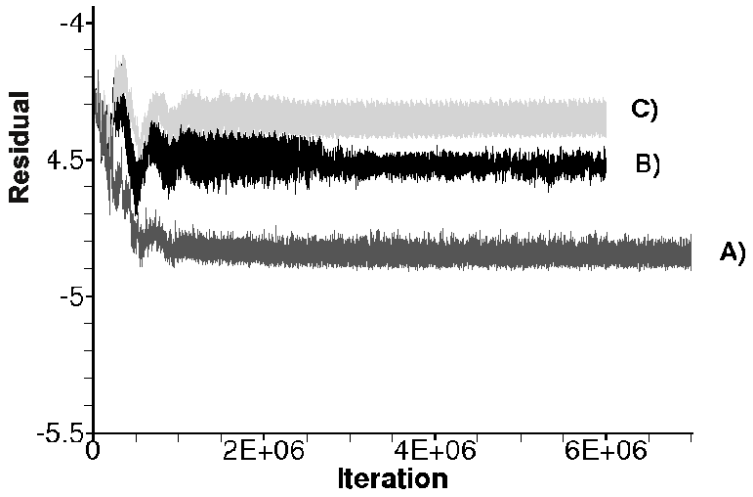

Figure 5: Convergence to the steady state solution. Computed in domain D_1 with: A) *Full system*, B) *Adiabatic system*, C) *Iso-energetic system*.

where $\frac{\hat{u}_{\max}}{\hat{c}_\infty} = 0.535$ ($\hat{u}_{max} = 183.5$ ms^{-1}) at g=1.002 mm (opening phase). *Adiabatic system* and *Iso-energetic system* (Figs. 7, 8) have same absolute maximum velocity ratio during one vibration period $\frac{\hat{u}_{\max}}{\hat{c}_\infty} = 0.199$ ($\hat{u}_{max} = 68.2$ ms^{-1}) at $g = 0.993$ mm and $g = 1.09$ mm respectively, during closing phase.

5. Discussion and conclusions

Three governing systems for flow of viscous compressible fluid based on Navier-Stokes equations for laminar flow are tested. Numerical solutions showed similar pattern of the flow fields computed with *Full*, *Adiabatic* and *Iso-energetic systems*. In unsteady simulations was possible to detect a "Coandă phenomenon" and large-scale vortices in the flow field patterns. The direction of the jet is independent on the coarseness of mesh but depends on the geometry of the channel, on the type of mesh in the domain, on the computational scheme [8] and on the governing system of flow. A similar generation of large-scale vortices, vortex convection and diffusion, jet flapping, and general flow patterns were experimentally obtained in physical models of the vocal folds by using Particle Image Velocimetry method in [9].

In next time we consider analyze spectrum of acoustic pressure found near the outlet of domain D_1 and to compute the similar case by model of incompressible Navier-Stokes equations and to use extension to 3D case.

Acknowledgements

This contribution was partially supported by Research Plans MSM 6840770010, GAČR P101/11/0207, 201/08/0012 and P101/10/1329.

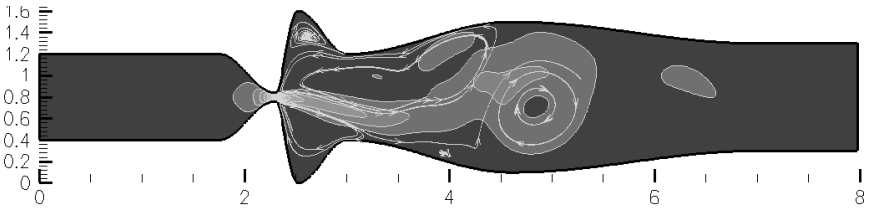

(a) $t = 30$ ms, $g = 1.6$ mm, $\frac{\hat{u}_{\max}}{\hat{c}_\infty} = 0.162$ (55.6 ms^{-1})

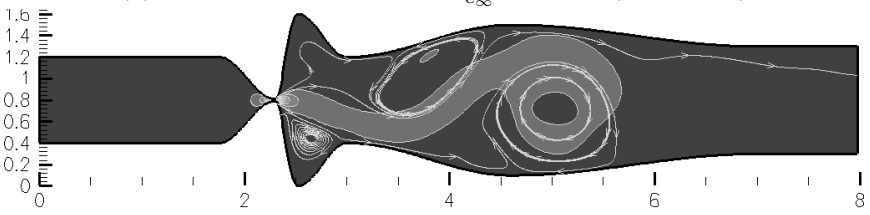

(b) $t = 32.5$ ms, $g = 0.4$ mm, $\frac{\hat{u}_{\max}}{\hat{c}_\infty} = 0.236$ (80.9 ms^{-1})

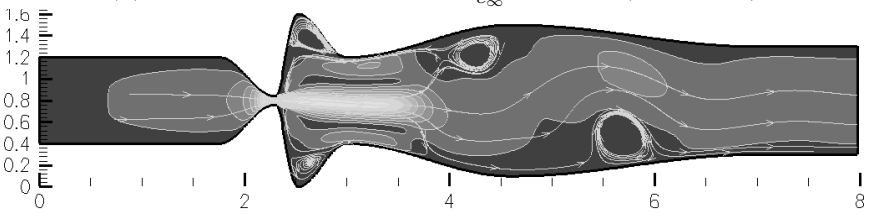

(c) $t = 35$ ms, $g = 1.6$ mm, $\frac{\hat{u}_{\max}}{\hat{c}_\infty} = 0.370$ (126.9 ms^{-1})

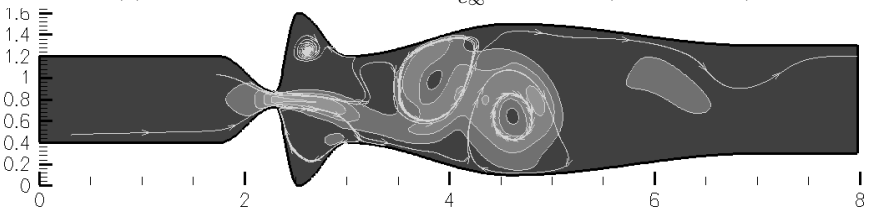

(d) $t = 37.5$ ms, $g = 2.8$ mm, $\frac{\hat{u}_{\max}}{\hat{c}_\infty} = 0.097$ (33.3 ms^{-1})

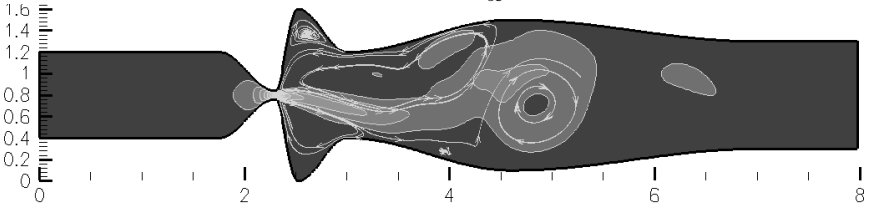

(e) $t = 40$ ms, $g = 1.6$ mm, $\frac{\hat{u}_{\max}}{\hat{c}_\infty} = 0.162$ (55.6 ms^{-1})

Figure 6: The unsteady numerical solution of the airflow in D_1 computed with *Full system* - $\hat{f} = 100$ Hz, $\frac{\hat{u}_\infty}{\hat{c}_\infty} = 0.012$, $\mathrm{Re}_\infty = 4481$, $p_2 = 1/\kappa$, 450×100 cells. Data computed during the fourth oscillation cycle. Results are mapped by iso-lines of velocity ratio and by streamlines.

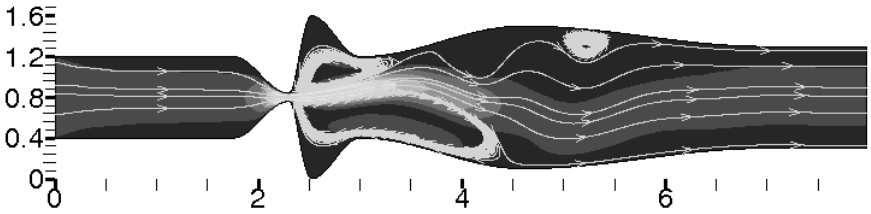

(a) $t = 30$ ms, $g = 1.6$ mm, $\frac{\hat{u}_{\max}}{\hat{c}_\infty} = 0.167$ (57.2 ms^{-1})

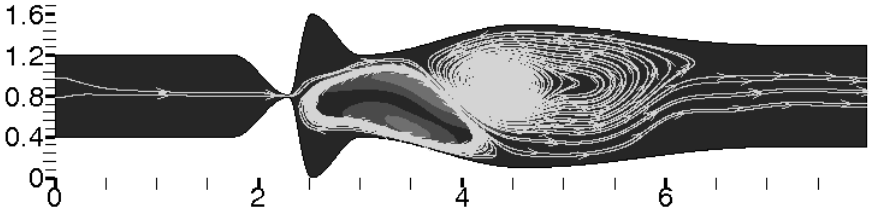

(b) $t = 32.5$ ms, $g = 0.4$ mm, $\frac{\hat{u}_{\max}}{\hat{c}_\infty} = 0.032$ (10.9 ms^{-1})

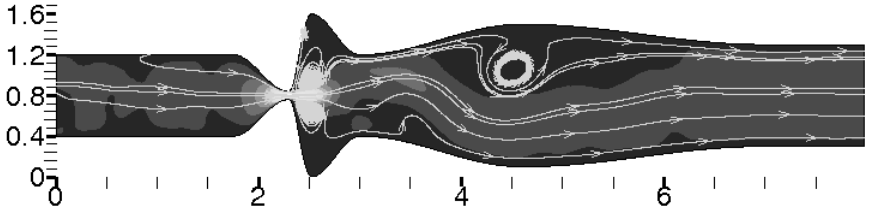

(c) $t = 35$ ms, $g = 1.6$ mm, $\frac{\hat{u}_{\max}}{\hat{c}_\infty} = 0.171$ (58.6 ms^{-1})

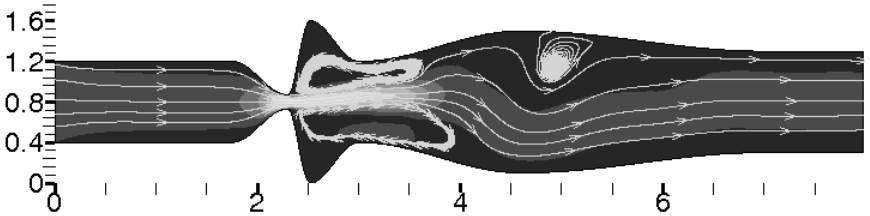

(d) $t = 37.5$ ms, $g = 2.8$ mm, $\frac{\hat{u}_{\max}}{\hat{c}_\infty} = 0.093$ (31.9 ms^{-1})

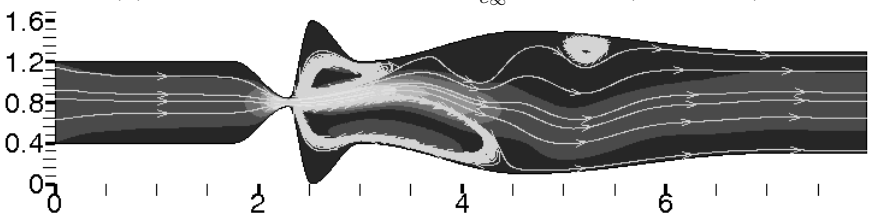

(e) $t = 40$ ms, $g = 1.6$ mm, $\frac{\hat{u}_{\max}}{\hat{c}_\infty} = 0.167$ (57.2 ms^{-1})

Figure 7: The unsteady numerical solution of the airflow in D_1 computed with *Adiabatic system* - $\hat{f} = 100$ Hz, $\frac{\hat{u}_\infty}{\hat{c}_\infty} = 0.012$, $\mathrm{Re}_\infty = 4481$, $p_2 = 1/\kappa$, 450×100 cells. Data computed during the fourth oscillation cycle. Results are mapped by iso-lines of velocity ratio and by streamlines.

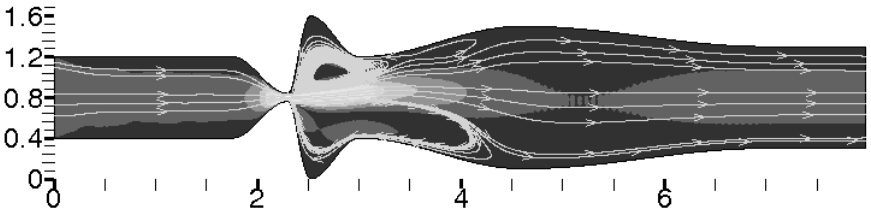

(a) $t = 30$ ms, $g = 1.6$ mm, $\frac{\hat{u}_{\max}}{\hat{c}_\infty} = 0.163$ (55.9 ms^{-1})

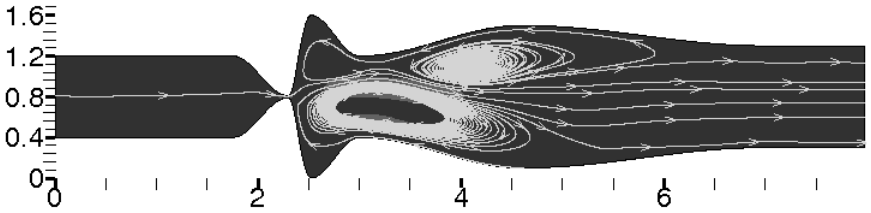

(b) $t = 32.5$ ms, $g = 0.4$ mm, $\frac{\hat{u}_{\max}}{\hat{c}_\infty} = 0.030$ (10.3 ms^{-1})

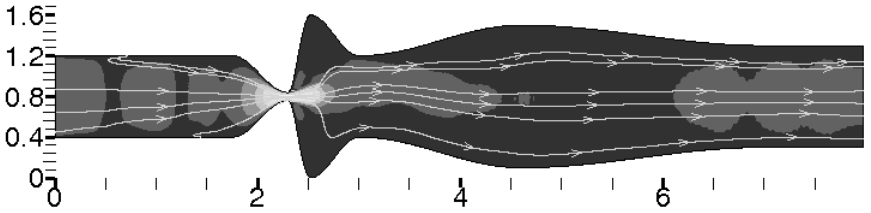

(c) $t = 35$ ms, $g = 1.6$ mm, $\frac{\hat{u}_{\max}}{\hat{c}_\infty} = 0.159$ (54.5 ms^{-1})

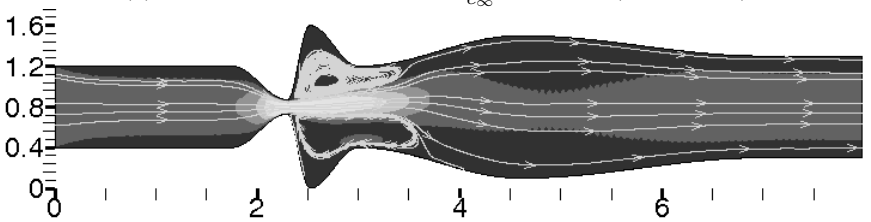

(d) $t = 37.5$ ms, $g = 2.8$ mm, $\frac{\hat{u}_{\max}}{\hat{c}_\infty} = 0.097$ (33.3 ms^{-1})

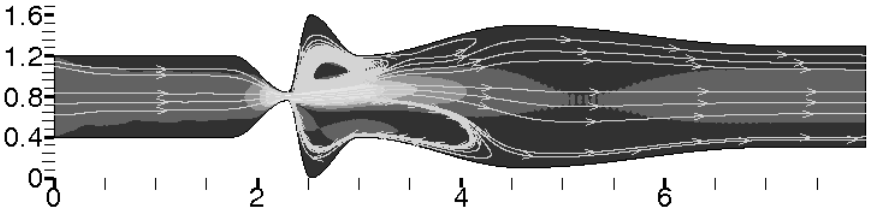

(e) $t = 40$ ms, $g = 1.6$ mm, $\frac{\hat{u}_{\max}}{\hat{c}_\infty} = 0.163$ (55.9 ms^{-1})

Figure 8: The unsteady numerical solution of the airflow in D_1 computed with *Isoenergetic system* - $\hat{f} = 100$ Hz, $\frac{\hat{u}_\infty}{\hat{c}_\infty} = 0.012$, $\mathrm{Re}_\infty = 4481$, $p_2 = 1/\kappa$, 450×100 cells. Data computed during the fourth oscillation cycle. Results are mapped by iso-lines of velocity ratio and by streamlines.

References

[1] Titze, I. R.: *Principles of voice production*. National Center for Voice and Speech, Iowa City, 2000. ISBN 0-87414-122-2.

[2] Titze, I. R.: *The myoelastic aerodynamic theory of phonation*. National Center for Voice and Speech, Iowa City, 2006. ISBN 0-87414-122-2.

[3] Zöner, S., Kalteenbacher, M., Mattheus, W., and Brücker, C.: Human phonation analysis by 3d aero-acoustic computation. In: *Proceedings of the International Conference on Acoustic NAG/DAGA*, pp. 1730–1732. Rotterdam, 2009.

[4] Fürst, J., Janda, M., and Kozel, K.: Finite volume solution of 2D and 3D Euler and Navier- Stokes equations. In: J. Neustupa, P. Penel (Eds.), *Mathematical fluid mechanics*, pp. 173-194, Berlin, 2001, ISBN 3-7643-6593-5.

[5] Punčochářová - Pořízková, P., Horáček, J., Kozel, K., and Fürst, J.: Numerical simulation of unsteady compressible low Mach number flow in a channel. Engineering mechanics **17** (2) (2010), 83–97.

[6] Honzátko, R., Horáček, J., and Kozel, K.: Solution of inviscid incompressible flow over a vibrating profile. In: M. Beneš, M. Kimura, and T. Nataki (Eds.), *COE Lecture notes*, vol. 3, pp. 26–32. Kyushu University, 2006. ISSN 1881-4042.

[7] Jameson, A., Schmidt, W., and Turkel, E.: Numerical solution of the Euler equations by the finite volume methods using Runge-Kutta time-stepping schemes. AIAA (1981), 81–125.

[8] Pořízková, P., Kozel, K., and Horáček, J.: Numerical tests of flow in human vocal tract. In: *Interaction of Dynamic Systems with Surroundings and Systems with Feedbacks. Prague: Institute of Thermomechanics, AS CR, v.v.i.*, pp. 79–86, 2010. ISBN 978-80-87012-29-1.

[9] Horáček, J., Šidlof, P., Uruba, V., Veselý, J., Radolf, V., and Bula, V.: PIV Measurement of flow-patterns in human vocal tract model. In: *Proceedings of the International Conference on Acoustic NAG/DAGA*, pp. 1737–1740. Rotterdam, 2009.